Characterization of the electron propagator with a *GW*-like self-energy in closed-shell atoms

S. Verdonck,[1] D. Van Neck,[1] P. W. Ayers,[2] and M. Waroquier[1]
[1]*Laboratory of Theoretical Physics, Ghent University, Proeftuinstraat 86, B-9000 Gent, Belgium*
[2]*Department of Chemistry, McMaster University, Hamilton, Ontario, Canada L8S4M1*
(Received 24 May 2006; published 6 December 2006)

The electron propagator is calculated for a set of closed-shell atoms using *GW*-like self-energies that contain the coupling of single-particle degrees of freedom with excited states in the framework of the random phase approximation. The effect of including exchange diagrams is investigated. Calculations are performed in the Hartree-Fock (HF) basis of the neutral atom. The HF continuum is taken into account using a discretization procedure, and the basis set limit is estimated using a systematic increase of basis set size. We check the approximation of taking the self-energy diagonal in the HF basis, and to what extent the extended Koopman's theorem is fulfilled using an approximate self-energy. Finally we try to model the information contained in the propagator in terms of a functional containing Hartree-Fock quantities and demonstrate the feasibility of simultaneously reproducing the correlation and ionization energy of an underlying *ab initio* model.

DOI: 10.1103/PhysRevA.74.062503 PACS number(s): 31.10.+z, 31.15.Ar

I. INTRODUCTION

It is well known that *ab initio* treatments of electronic systems become unworkable for sufficiently complex systems. In many modern applications the Kohn-Sham formulation [1] of density functional theory (DFT) [2], where only single-particle equations must be solved in a self-consistency loop, is the only feasible approach. There is therefore continuing interest, not only in developing new and more accurate functionals, but also in studying conceptual improvements and extensions to the DFT framework. In particular there is room for improvement in the description of long-range (van der Waals) forces and dissociation processes [3–9]. More generally one could say that the present DFT can handle short-range interelectronic correlations quite well, but often fails when dealing with near-degenerate systems characterized by a small particle-hole gap.

Microscopic theories offer some guidance in the development of extensions to DFT. Orbital dependent functionals can be constructed using many-body perturbation theory (MBPT) [10,11], though the spirit of DFT is somewhat violated [12] since one must perform a MBPT calculation for each system. In fact, the lack of a systematic improvement in DFT methods is addressed by the recent development of general *ab initio* DFT [13–16]. In this approach one considers a perturbative expansion (e.g., MBPT or coupled cluster) that generates the exact ground-state wave function from a chosen reference determinant. Requiring that the correction to the density vanishes at a certain level of perturbation theory allows one to construct the corresponding approximation to the Kohn-Sham potential. While highly interesting from a theoretical point of view, it is again unclear how much is gained by reformulating the perturbation techniques in terms of DFT quantities, though it is claimed that in low orders (second-order MBPT) significant improvements can be made over MP2 results evaluated with Hartree-Fock orbitals [15].

Among various *ab initio* approaches, one can expect the relationship between DFT and the propagator or Green's function (GF) formulation of many-body theory [17,18] to be especially fruitful [19]. The Dyson equation of GF theory is essentially also a single-particle equation, with the electronic self-energy appearing as a (complex and energy-dependent) potential that treats correlation effects exactly. The resulting electron propagator (or its imaginary part, the spectral function) contains most of the relevant information, including the total binding energy, the one-body density matrix, and the ionization energies and electron affinities. The use of GF theory in electronic structure problems has a long history (see, e.g., Refs. [20–25] for reviews and general papers). The link between GF theory and DFT has been explored through the Sham-Schlüter equations [26].

An alternative approach to the *ab initio* DFT route would be to concentrate directly on the electron spectral function for a number of systems, identify the components that are universal (i.e., not depending on the external potential), and model these in terms of functionals. The present paper is a step in this direction and demonstrates that it is feasible, within this framework, to reproduce the results of a GF calculation with an underlying microscopic model for the self-energy.

The microscopic model used in this paper has a self-energy of the *GW* type [27]. That is, it treats the coupling of single-particle states with the two-particle–one-hole ($2p1h$) and one-particle–two-hole ($1p2h$) space, including partial diagonalization in the $1p1h$ space through the random phase approximation (RPA). This allows for possible collective effects on the atomic excited states. Nonrelativistic GF calculations have been performed for the neutral closed-shell atoms He, Be, Ne, Mg, Ar, Ca, Zn, and Kr. While the lack of relativistic effects is of course inappropriate for the heaviest atoms, the results are still useful for identifying trends in nonrelativistic Coulombic systems.

Apart from the above motivation, there are several interesting aspects in these calculations. In previous papers [28–30] the second-order self-energy was treated, with emphasis on the self-consistency between the propagator and the self-energy. The present paper extends this study by examining the higher-order diagrams related to the RPA description of the excited states, though we did not attempt to

do this in a self-consistent fashion. We also look at the influence of the exchange diagrams in the particle-hole channel. In the GF description of the electron gas and periodic systems the role of exchange is still debated in connection with issues of self-consistency [31–33], but it does not seem to have been studied in any detail for finite systems. Finally, the closed-shell atoms are simple enough (spherical symmetry) to allow a quasiexact treatment of the single-particle continuum, a feature that is lacking when finite basis sets are used. This is in accord with the idea that functionals should be parametrized in the basis set limit [34].

The choice for *GW*-like self-energies is primarily made for convenience, as it allows the use of large basis sets. More accurate ionization energies would be obtained with increasingly sophisticated self-energy models, e.g., using the algebraic diagrammatic construction (ADC) method [35,36] where an approximate three-particle propagator is constructed, though this seems only feasible in small model spaces.

The paper is organized as follows. In Sec. II, the formalism of propagator theory is briefly summarized, introducing the RPA and the *GW* self-energy. Numerical details of the calculation are discussed in Sec. III, including the method of continuum discretization and convergence issues related to basis set size. The importance of such a convergence study is emphasized by comparing the results in Ref. [28], obtained with a self-consistent second-order self-energy, to those of a recent calculation [37]. We also test, at the second-order level, in how far the approximation of taking the self-energy diagonal in the Hartree-Fock (HF) basis is justified, and whether the extended Koopman's theorem [38–41] still holds when using a nonexact self-energy. Section IV contains a detailed analysis of the numerical results for the single-particle properties and correlation energies. In Sec. V A, the theoretical outline is given of a method for treating electron correlations. The method relies on the decomposition of the spectral function in its quasiparticle part and a small correlation part, where the latter should be modeled by means of a functional. An example of how the decomposition can be achieved is worked out in Sec. V B. In Sec. V C, a functional is constructed that reproduces the *ab initio* results of Sec. IV. Finally, a summary and some conclusions are formulated in Sec. VI.

Atomic units are used throughout the paper.

II. THEORY

A. Dyson equation

The theoretical framework used in this study is that of propagator theory, where the single-particle (sp) propagator is the object of interest, instead of the many-body wave function. The sp propagator is defined in configuration and energy space as

$$G(\alpha,\beta;E) = \langle \Psi_0^N | a_\alpha \frac{1}{E-(\hat{H}-E_0^N)+i\eta} a_\beta^\dagger + a_\beta^\dagger \frac{1}{E+(\hat{H}-E_0^N)-i\eta} a_\alpha | \Psi_0^N \rangle, \quad (1)$$

where $\alpha,\beta,\ldots$, label the elements of a complete orthonormal basis set of sp states, the second-quantization operators a_α ($a_\beta^\dagger$) remove (add) a particle in state α (β), and $\eta>0$ is an infinitesimal convergence parameter. The exact ground state of the N-electron system is denoted by $|\Psi_0^N\rangle$ and its energy by E_0^N. The Hamiltonian $\hat{H}$ reads

$$\hat{H} = \hat{H}_0 + \hat{V}, \quad (2)$$

where $\hat{H}_0$ contains the kinetic energy and electron-nucleus attraction, and $\hat{V}$ is the interelectron repulsion, with

$$\langle \alpha\beta | V | \gamma\delta \rangle_{as} = \langle \alpha\beta | V | \gamma\delta \rangle - \langle \alpha\beta | V | \delta\gamma \rangle \quad (3)$$

its antisymmetrized matrix element.

The sp propagator in Eq. (1) can be written alternatively in its Lehmann representation,

$$G(\alpha,\beta;E) = \sum_m \frac{\langle \Psi_0^N | a_\alpha | \Psi_m^{N+1} \rangle \langle \Psi_m^{N+1} | a_\beta^\dagger | \Psi_0^N \rangle}{E-(E_m^{N+1}-E_0^N)+i\eta} + \sum_n \frac{\langle \Psi_0^N | a_\beta^\dagger | \Psi_n^{N-1} \rangle \langle \Psi_n^{N-1} | a_\alpha | \Psi_0^N \rangle}{E+(E_n^{N-1}-E_0^N)-i\eta}, \quad (4)$$

where the $|\Psi_m^{N+1}\rangle$, $|\Psi_n^{N-1}\rangle$ are the eigenstates, and E_m^{N+1}, E_n^{N-1} the eigenenergies, in the $(N\pm1)$-electron system. The poles of the propagator therefore reflect the electron affinities and ionization energies, and are located at $\mathcal{A}_m^N = E_m^{N+1} - E_0^N$ (addition domain) and at $\mathcal{I}_n^N = E_0^N - E_n^{N-1}$ (removal domain).

The propagator holds enough information to calculate any one-body observable of interest. In addition, the total energy (in case of a Hamiltonian with at most two-body interactions) is also known through the Migdal-Galitskii sum rule, expressed in matrix form as

$$E_0^N = \frac{1}{2}\int \frac{dE}{2\pi i} e^{i\eta E} \mathrm{Tr}\{([H_0]+E)[G(E)]\}. \quad (5)$$

The sp propagator can be determined through Dyson's equation,

$$[G(E)] = [G^{(0)}(E)] + [G^{(0)}(E)][\Sigma(E)][G(E)]. \quad (6)$$

In this equation, $G^{(0)}(E)$ represents the sp propagator of the noninteracting system with Hamiltonian $\hat{H}_0$, and $G(E)$ that of the complete Hamiltonian $\hat{H}$. The (irreducible) self-energy $\Sigma(E)$ has a perturbative expansion as a power series in the interelectron Coulomb repulsion $\hat{V}$. Each term in the series also contains a number of noninteracting propagators. A self-consistent Green's function approach involves a regrouping of the series, in which the self-energy is expressed in terms of the dressed propagators $G(E)$, rather than the noninteracting ones. To first order in $\hat{V}$ this amounts to Hartree-Fock. The second-order self-consistent approach has been studied in Ref. [28]. In Fig. 1 the corresponding self-energy is represented diagrammatically, as well as the structure of the lowest-order diagrams that are generated when the self-consistent self-energy is expanded in terms of HF propagators.

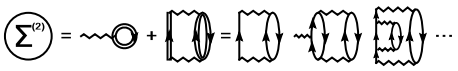

FIG. 1. Diagrams for the self-consistent second-order self-energy. Single fermion lines represent the HF propagator, double lines the self-consistent propagator. The antisymmetrized interaction matrix elements are depicted as zigzag lines. On the right-hand side are the diagrams of the second and third order, and a representative fourth-order diagram, that are generated when the self-energy is expanded in terms of the HF propagator.

Other approximations to the self-energy can be constructed by summing a particular class of diagrams to infinite order in $\hat{V}$. For the high-density electron gas the relevant class contains the ring diagrams. Note that the higher-order ring diagrams are not generated in the self-consistent second-order self-energy. The explicit summation of ring diagrams is known as the random phase approximation (RPA), and the corresponding G_0W_0 self-energy takes into account screening corrections to the bare Coulomb force. The self-consistent GW version is able to generate excellent correlation energies in the electron gas, but has some nonrealistic features (e.g., the damping of plasmon-related structures) [31–33]. These probably require a more sophisticated treatment of the exchange part of the particle-hole interaction.

B. Polarization propagator

For the finite systems treated in the present paper we use a self-energy approximation that incorporates RPA collective particle-hole excitations. The excited states in the N-electron system can be described by means of the polarization propagator

$$\Pi(\alpha,\beta^{-1};\gamma,\delta^{-1};E)=\sum_{n>0}\frac{X^n_{\alpha\beta}(X^n_{\gamma\delta})^*}{E-\mathcal{E}_n+i\eta}-\sum_{n>0}\frac{(Y^n_{\alpha\beta})^*Y^n_{\gamma\delta}}{E+\mathcal{E}_n-i\eta}, \tag{7}$$

where $\mathcal{E}_n=E^N_n-E^N_0$ are the excitation energies, and the transition amplitudes read

$$X^n_{\alpha\beta}=\langle\Psi^N_0|a^\dagger_\beta a_\alpha|\Psi^N_n\rangle,\quad Y^n_{\alpha\beta}=\langle\Psi^N_0|a^\dagger_\alpha a_\beta|\Psi^N_n\rangle=X^n_{\beta\alpha}. \tag{8}$$

The RPA approximation to the polarization propagator is shown diagrammatically in Fig. 2. We will consider two different polarization propagators: RPA proper, where only the direct part of the ph interaction is included, and G (generalized) RPA where both the direct and exchange matrix elements enter. The restriction to only direct matrix elements is very natural for the electron gas, as they are dominant for $1p1h$ excitations with small total momentum. For a finite

FIG. 2. Diagrammatic equation for the RPA and GRPA polarization propagators. The dashed (zigzag) line represents a direct (antisymmetrized) Coulomb interaction matrix element. The fermion lines represent HF propagators.

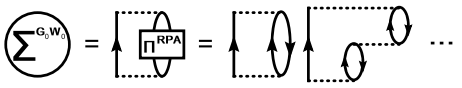

FIG. 3. Diagram for the G_0W_0 self-energy.

system one cannot say this *a priori*.

More explicitely, denoting the unoccupied (occupied) HF sp states with p (h), the transition amplitudes X^n_{ph} and Y^n_{ph} follow from the standard RPA eigenvalue problem,

$$\begin{pmatrix}A & B\\ B^* & A^*\end{pmatrix}\begin{pmatrix}X^n\\ Y^n\end{pmatrix}=\mathcal{E}_n\begin{pmatrix}1 & 0\\ 0 & -1\end{pmatrix}\begin{pmatrix}X^n\\ Y^n\end{pmatrix}, \tag{9}$$

where

$$A_{ph,p'h'}=\delta_{p,p'}\delta_{h,h'}(\epsilon^{\rm HF}_p-\epsilon^{\rm HF}_h)+\langle ph'|V|hp'\rangle,$$

$$B_{ph,p'h'}=\langle pp'|V|hh'\rangle \tag{10}$$

for RPA, whereas the antisymmetrized Coulomb matrix elements are taken for GRPA. The $\epsilon^{\rm HF}_\alpha$ are the HF sp energies, and the excited states correspond to the positive-energy solutions of Eq. (9), normalized as $1=\Sigma_{ph}(|X^n_{ph}|^2-|Y^n_{ph}|^2)$.

In practice, for the closed-shell systems under study spherical quantum numbers $\alpha\equiv n_a l_a m_{l_a} m_{s_a}$ are used, and the excited states are labeled by total orbital angular momentum L and total spin S.

C. Self-energy in $(G)G_0W_0$ approximation

The self-energy in the G_0W_0 approximation is shown diagrammatically in Fig. 3. Note that the HF part of the self-energy has been absorbed in the unperturbed propagators which represent HF sp states. The G_0W_0 self-energy contains intermediate states where the RPA excited states are coupled to HF sp states, and can be written as

$$\Sigma^{G_0W_0}(\alpha,\beta;E)=\sum_{p,n>0}\frac{U(\alpha,p;n)U^*(\beta,p;n)}{E-(\mathcal{E}_n+\epsilon^{HF}_p)+i\eta}+\sum_{h,n>0}\frac{U^*(h,\alpha;n)U(h,\beta;n)}{E+(\mathcal{E}_n-\epsilon^{HF}_h)-i\eta}, \tag{11}$$

in terms of the coupling vertex

$$U(\alpha,\beta;n)=\sum_{ph}(\langle\alpha h|V|\beta p\rangle X^n_{ph}+\langle\alpha p|V|\beta h\rangle Y^n_{ph}). \tag{12}$$

In both the RPA polarization propagator and the coupling vertex, only the direct term of the interaction is retained. It is also possible to use the GRPA polarization propagator and the full antisymmetrized interaction matrix elements in the coupling vertex of Eq. (12). This is henceforth called the G (generalized) G_0W_0 approximation, and the corresponding self-energy is depicted in Fig. 4.

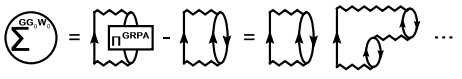

FIG. 4. Diagram for the GG_0W_0 self-energy.

As indicated in Fig. 4 the second-order diagram should be once subtracted, in order to compensate for double counting. A (partially) self-consistent scheme based on the same self-energy was referred to as G (generalized) GW in Ref. [42]. In this work, exchange diagrams are introduced by means of vertex corrections (instead of an antisymmetrized interaction), but upon expansion the same diagrammatical content is found. One should note that subtracting a diagram introduces poles with negative residue in the self-energy. This can lead to unphysical poles in the propagator, though it is seldom a problem for the ionization pole.

In most of the calculations the self-energy has been assumed diagonal in the HF basis,

$$\Sigma(\alpha,\beta;E) = \delta_{\alpha,\beta}\Sigma_{\alpha}(E). \tag{13}$$

We checked for a few cases (see also the discussion in the next section) that this introduces errors of 1–2 mH for the ionization energies, about the same error as finite basis set effects.

III. CALCULATIONAL DETAILS

A. Discretization of the continuum

The sp basis set to be used in the calculations should consist of the HF sp states in the neutral closed-shell atom. While the occupied states are discrete, all unoccupied HF states lie in the continuum. As it is technically hard to work with continuum states, we introduce discrete virtual orbitals in the manner of Ref. [28]. This amounts to first solving the HF problem for the occupied states, then adding to the HF mean field a parabolic potential wall $U(r)=\theta(r-r_w)c_w(r-r_w)^2$, placed at a distance r_w from the atomic center. The latter eigenvalue problem has a basis of discrete eigenstates. This basis is truncated by specifying the largest orbital angular momentum $l_{\max}$ and the number of unoccupied states for each l. Finally the HF problem (without the parabolic potential wall) is solved again in the truncated basis, yielding the sp basis set used in the calculations. Obviously the exact form of the auxiliary confining potential should not affect results, if a sufficiently large basis set is retained after truncation.

It was checked numerically for several cases that various parameters for the parabolic wall indeed yield the same basis set limit. The speed of convergence, however, can be very different, and reflects the range and accuracy of the sampling of the HF continuum. In addition, the potential wall cannot be too close to the center for the l values of the occupied states without spoiling the latter. As an example, in Fig. 5 the G_0W_0 ionization energy for Be is shown for two different confining potentials, as a function of increasing basis set size. Each incremental step represents addition of one higher l value with five virtual orbitals, while simultaneously increasing the number of virtual orbitals of the lower l by about 20%. The value $n=2$ corresponds to the size of the basis set used in Ref. [28]. For the radial wave functions with $l>0$, the upper curve in Fig. 5 uses a confining potential with $r_w=0$ and $c_w=5$, whereas the lower one uses $r_w=5$ and $c_w=5$ (expressed in atomic units).

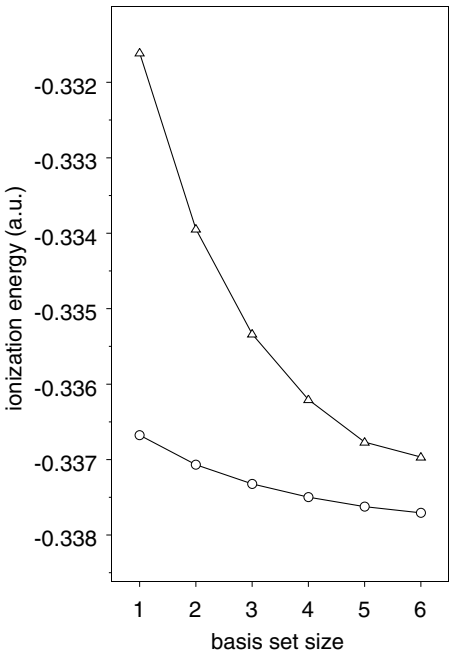

FIG. 5. Convergence behavior of the G_0W_0 ionization energy (a.u.) of Be for two different confining potentials, as a function of basis set size (see text).

Eventually, the same confining potentials were used as in the self-consistent second-order calculation of Ref. [28] (see Table I).

The numerical treatment of the continuum states in a finite system can be troublesome. Note that this issue was recently investigated in Ref. [43], where small molecules were treated with a partially self-consistent GW self-energy using a periodic code and a supercell technique to describe isolated molecules. This led to extremely poor convergence in terms of the number of scattering states retained in the model space. Such difficulties, however, were not encountered with the discretization of the continuum in the present work.

B. Convergence issues

For the default calculations the size of the basis sets (see Table I) was taken the same as in Ref. [28], where it yielded convergence to about 1 mH, for the ionization energy with the second-order self-energy. We checked that the same holds for the $(G)G_0W_0$ ionization energies in the present paper.

The total energies converge much slower than the ionization energies. This is due to the laborious description of the interelectronic cusp when expanding in noninteracting wave functions [44,45], and the fact that cusp effects tend to cancel for the ionization energy (being a difference of two energies). In order to estimate contributions to the total energy missing due to basis set truncation, we studied the convergence properties when performing systematic basis set increases in the manner described above. Numerically one finds that the corresponding changes to the energy behave in a very smooth way, with a decrease that is slower than

TABLE I. Confining potentials $U(r)=\theta(r-r_w)c_w(r-r_w)^2$, and number of occupied (N_{occ}) and unoccupied (N_{vir}) orbitals for the basis sets used in the default calculation. Entries for each l value read (N_{occ}-N_{vir}-r_w). The parameter c_w has the same value ($c_w=5$) in all cases.

l	He	Be	Ne	Mg	Ar	Ca	Zn	Kr
0	1-20-3	2-20-11	2-10-2	3-20-10	3-20-1	4-25-12	4-15-7	4-15-7
1	0-15-0	0-20-5	1-20-4	1-20-7	2-25-3	2-25-7	2-25-10	3-25-10
2	0-8-0	0-10-5	0-10-0	0-20-5	0-20-0	0-20-5	1-3-4	1-15-5
3	0-5-0	0-10-5	0-10-0	0-15-3	0-10-0	0-10-3	0-15-0	0-15-0
4	0-5-0	0-5-5	0-5-0	0-10-1	0-10-0	0-10-1	0-15-0	0-15-0
5	0-5-0	0-5-5	0-5-0	0-5-0	0-5-0	0-5-0	0-15-0	0-15-0
6	0-5-0	0-5-5	0-5-0	0-5-0	0-5-0	0-5-0	0-10-0	0-10-0
7		0-5-5					0-5-0	0-5-0
8							0-5-0	0-5-0

exponential but faster than an inverse power law. By extrapolating in both ways one obtains upper and lower bounds to the basis set limit. For the lighter atoms, the numerical tables below contain these bounds, together with the result of the default basis set size of Table I. For the heavier atoms such a convergence study was not possible, but similar basis set truncation errors should be expected.

In order to check the reliability of these bounds we also applied the extrapolation scheme to the MP(2) energies obtained with the same basis sets. The resulting upper an lower bounds are shown in Table II and Table VI; the interval contains the quasiexact MP(2) basis set limit for He to Ar obtained in Ref. [45], except for Be (by less than 2 mH). As expected, the same extrapolation procedure performed on the ionization energies yields corrections that are much smaller.

The issue of basis set truncation errors is important, especially when comparing GF results by different authors. As an example, Table II contains correlation and ionization energies obtained with the second-order self-energy, evaluated both with HF propagators and in self-consistent GF theory. The self-consistent version, first applied to atoms in Ref. [28] and more recently in Ref. [37], is quite involved and does not allow a very large number of sp orbitals.

For the correlation energies $[E_0^N-E_0^N(\mathrm{HF})]$ similar qualitative trends are observed [e.g., the near equivalence of the MP(2) calculation with the self-consistent energies], but the small size of the basis sets used in Ref. [37] precludes a direct comparison. This can also be appreciated by comparing the MP(2) values. For Ne, e.g., the MP(2) limit value is −0.388 H [45]. Our standard basis yields −0.338 H. The value obtained in Ref. [37] by evaluating the Luttinger-Ward functional with HF propagators is expected to coincide with the MP(2) value, and yields only −0.286 H.

For the ionization energies the agreement, as expected, is much better, though one still finds deviations of 20 mH (in the self-consistent result for Ne). Comparing with the extrapolated values in Table II, it is again plausible that this is due to the limited size of the basis sets in Ref. [37]. Apart from basis set differences, the ionization energies in Ref. [37] were calculated on the basis of the extended Koopman's theorem or EKT (see Refs. [38–41] for a recent numerical application), as the lowest eigenvalue λ of the generalized eigenvalue problem $[M^{(-)}]u=\lambda[N^{(-)}]u$, in terms of the removal energy matrix $[M^{(-)}]$ and one-body density matrix $[N^{(-)}]$,

TABLE II. Correlation and ionization energies (a.u.) obtained with the second-order self-energy, evaluated non-self-consistently $[\Sigma^{(2)}(G_{\mathrm{HF}})]$, and self-consistently $[\Sigma^{(2)}(G)]$. Values as obtained by Dahlen *et al.* (Ref. [37]) and by Van Neck *et al.* (Ref. [28]). The $\Sigma^{(2)}(G_{\mathrm{HF}})$ values in Ref. [28] were recalculated for the present work, and the extrapolation bounds (see text) are indicated between brackets. The corresponding MP(2) correlation energies are also given. The column labeled $E_{LW}(G_{\mathrm{HF}})$ corresponds to the MP(2) values in Ref. [37].

	Correlation energies						Ionization energies			
	Ref. [37]			Ref. [28] and present work			Ref. [37]		Ref. [28] and present work	
	$\Sigma^{(2)}(G_{\mathrm{HF}})$	$\Sigma^{(2)}(G)$	$E_{\mathrm{LW}}(G_{\mathrm{HF}})$	$\Sigma^{(2)}(G_{\mathrm{HF}})$	$\Sigma^{(2)}(G)$	MP(2)	$\Sigma^{(2)}(G_{\mathrm{HF}})$	$\Sigma^{(2)}(G)$	$\Sigma^{(2)}(G_{\mathrm{HF}})$	$\Sigma^{(2)}(G)$
He	−0.0396	−0.0352	−0.0352	−0.037 [−0.0356,−0.0344]	−0.037	−0.0368 [−0.0374,−0.0372]	0.9059	0.9017	0.905 [0.9051,0.9053]	0.906
Be	−0.0934	−0.0681	−0.0677	−0.060 [−0.0652,−0.0640]	−0.055	−0.0615 [−0.0745,−0.0730]	0.3275	0.3130	0.330 [0.3301,0.3302]	0.320
Ne	−0.2509	−0.2869	−0.2862	−0.160 [−0.1594]	−0.339	−0.338 [−0.389,−0.369]	0.7363	0.7412	0.745 [0.7475,0.7483]	0.763
Mg	−0.3133	−0.2951	−0.2947	−0.134 [−0.159,−0.154]	−0.331	−0.331 [−0.446,−0.383]	0.2605	0.2548	0.276 [0.2764,0.2766]	0.274

TABLE III. Energies (a.u.) of low-lying excited states in He and Ne obtained in GRPA. The first column contains the dominant *ph* configuration. In the last two columns, the *LS*-averaged GRPA values are compared with the *J*-averaged experimental ones [49].

ph	$E(L^{\Pi}S)$	Average	Experimental
	He		
$1s2s$	$0.776(0^+0)$, $0.724(0^+1)$	0.737	0.736
$1s2p$	$0.797(1^-0)$, $0.780(1^-1)$	0.784	0.773
$1s3s$	$0.858(0^+0)$, $0.846(0^+1)$	0.849	0.837
	Ne		
$2p3s$	$0.674(1^-0)$, $0.660(1^-1)$	0.664	0.614
$2p3p$	$0.755(0^+0)$, $0.717(0^+1)$, $0.740(1^+0)$, $0.740(1^+1)$, $0.739(2^+0)$, $0.733(2^+1)$	0.735	0.684
$2p4s$	$0.782(1^-0)$, $0.779(1^-1)$	0.780	0.724

$$N^{(-)}_{\alpha,\beta} = \int \frac{dE}{2\pi i} e^{i\eta E} G(\alpha,\beta;E) = \langle \Psi^N_0 | a^\dagger_\beta a_\alpha | \Psi^N_0 \rangle,$$

$$M^{(-)}_{\alpha,\beta} = \int \frac{dE}{2\pi i} e^{i\eta E} EG(\alpha,\beta;E) = \langle \Psi^N_0 | a^\dagger_\beta [a_\alpha, \hat{H}] | \Psi^N_0 \rangle. \tag{14}$$

The ionization energies in Ref. [28], on the other hand, were obtained directly by solving Dyson's equation, under the assumption that the self-energy is diagonal in the HF basis.

In order to assess these different methods a test calculation for Ne was performed with the non-self-consistent second-order self-energy, without the diagonality assumption. The ionization energy calculated directly from the Dyson equation (0.747 H) was indeed found to coincide with the EKT value, suggesting that EKT also holds for a simple approximate self-energy. At the same time, the ionization pole is also close to the default result (0.745 H) calculated by solving Dyson's equation with a diagonal approximation for the self-energy. Obviously the EKT, which relies on the asymptotics in coordinate space, does not hold for a diagonal approximation. We did check that for average quantities such as the mean-removal energy, $\mathrm{Tr}[M^{(-)}_{l=1}]$, or occupation number, $\mathrm{Tr}[N^{(-)}_{l=1}]$, of an $l=1$ electron in Ne, the diagonal (nondiagonal) results are again very close, −0.9620 H (−0.9638 H) and 0.9963 (0.9965), respectively.

IV. NUMERICAL RESULTS

A. (G)RPA excited states

In Table III, the energies of a few low-lying $1p1h$ excited states in He and Ne, as obtained in the GRPA, are compared with the experimental ones. Note that in HF on the neutral atom no bound p (unoccupied) orbitals exist; the *ph* spectrum has no discrete excited states, but a continuum starting at $-\epsilon^{\mathrm{HF}}_h$. The same holds in RPA, since the direct *ph* interaction is repulsive. Only in GRPA, where the attractive *ph* exchange term is included, do discrete excited states appear that form a Rydberg series as seen experimentally. This can easily be seen [46] by considering a sub-block of the GRPA A-matrix in Eq. (9) formed by the *ph* states with the same h, i.e.,

$$H^{(h)}_{p,p'} = A_{ph,p'h} = \delta_{p,p'}(\epsilon^{\mathrm{HF}}_p - \epsilon^{\mathrm{HF}}_h) + \langle ph|V|hp'\rangle_{as}. \tag{15}$$

Since the HF basis diagonalizes the HF Hamiltonian one has

$$\delta_{p,p'}\epsilon^{\mathrm{HF}}_p = \langle p|H_0|p'\rangle + \sum_{h''} \langle ph''|V|p'h''\rangle_{as}, \tag{16}$$

so that

$$H^{(h)}_{p,p'} = -\delta_{p,p'}\epsilon^{\mathrm{HF}}_h + \langle p|H_0|p'\rangle + \sum_{h''(\neq h)} \langle ph''|V|p'h''\rangle_{as}. \tag{17}$$

The matrix $H^{(h)}$ clearly represents a sp Hamiltonian where the HF mean field of the neutral atom is changed to an ionic mean field by canceling the contribution of orbital h. Hence the appearance of the Rydberg sequence in GRPA, since the ionic mean field goes asymptotically like $-1/r$. Similar considerations applied to RPA show that to the neutral atom HF mean field a repulsive term (on the diagonal) $\langle ph|V|hp\rangle$ is added, which cannot give rise to a discrete *ph* spectrum. The appearance of an ionic mean field for the unoccupied states is the most important collective effect in *ph* space, which otherwise shows little mixing among states with different h, and provides the microscopic underpinning for use of the V^{N-1} potential [47].

For the noble gases the GRPA spectrum is in reasonable agreement with experiment when (since we do not use spin-orbit coupling) averaged energies are compared, i.e., the *J*-averaged experimental energies are compared with the *LS*-averaged GRPA energies, see Table III.

For Be and Ca the GRPA equation has a complex solution in the $L^\pi = 1^-, S=1$ channel. This reflects an instability (due to the small *ph* gap involved) of the closed-shell ground state against $2s^{-1}2p$ or $4s^{-1}4p$ particle-hole excitations, i.e., the closed-shell configuration is a poor starting point for a perturbative expansion. Similar remarks apply to Mg and Zn. In

TABLE IV. First ionization energies (a.u.), obtained with different self-energies: second-order non-self-consistently [$\Sigma^{(2)}(G_{\mathrm{HF}})$], self-consistently [$\Sigma^{(2)}(G)$], and G_0W_0. Extrapolation bounds are given between brackets. The column labeled (Expt.) contains the estimated nonrelativistic ionization energies from Ref. [48] for the atoms He through Ar; values for Ca through Kr are taken from Ref. [49].

	HF	$\Sigma^{(2)}(G_{\mathrm{HF}})$	$\Sigma^{(2)}(G)$ [28]	G_0W_0	GG_0W_0	Expt.
He	0.918	0.905	0.906	0.9089 [0.9096,0.9100]	0.878	0.9037
Be	0.309	0.330	0.320	0.3367 [0.3378,0.3383]	/	0.3426
Ne	0.850	0.745	0.763	0.801 [0.805,0.807]	0.714	0.7946
Mg	0.253	0.276	0.274	0.281 [0.282,0.283]	(0.412)	0.2808
Ar	0.590	0.578	0.585	0.595 [0.598,0.599]	0.609	0.583
Ca	0.195	0.224		0.224	/	0.2247
Zn	0.291	0.329		0.331	(0.484)	0.3452
Kr	0.524	0.526	0.560	0.536	0.548	0.5145

this case no complex solution occurs, but the lowest GRPA excitation energy is just above zero and cannot reproduce the experimental spectrum.

B. Comparison of G_0W_0 and GG_0W_0 results

In Table IV the first ionization energies of the eight atomic systems are shown, calculated with different self-energies. Note that even though the excitation spectrum is in principle continuous, the G_0W_0 ionization pole converges easily with increasing size of the discrete basis set. This is the same behavior as in a calculation with the second-order self-energy using the neutral atom HF propagator: discretization errors in the unoccupied states tend to be compensated by the interaction matrix elements. Similarly, one finds numerical convergence of the GG_0W_0 ionization pole long before the GRPA spectrum itself has converged.

The GG_0W_0 self-energy gives reasonable ionization poles only for the noble gases. Because of the GRPA instability no results are given in Table IV for Be and Ca. The ionization pole for Mg and Zn is badly off the mark, again because the GRPA spectrum is unrealistic. Even for the noble gases, it is interesting to note that the G_0W_0 ionization energies are considerably closer to the experimental value than GG_0W_0. Correlation effects, such as the shift from the ionization pole from its HF value, are severely overestimated in GG_0W_0. This points to the fact that exchange effects should be included in a more sophisticated way, and that superior results for the spectral function are obtained by leaving them out altogether (except at the level of the Fock mean field term).

C. Detailed G_0W_0 results

An overview of the sp properties obtained with the G_0W_0 self-energy is given in Table V. For comparison, the HF results, and the results obtained in Ref. [28] with the self-consistent second-order self-energy $\Sigma^{(2)}(G)$, are also listed. The table contains the position and strength of the dominant fragments in the spectral function. For the valence states the experimental energies come from Ref. [49] and the strengths (determined by electron momentum spectroscopy) from Refs. [49–52]. The single-particle energies for the core orbitals were taken from x-ray photoelectron spectroscopy [53]. The G_0W_0 description of the valence states is on the whole remarkably good, and an improvement on the $\Sigma^{(2)}(G)$ results. For the more deeply bound sp states, both are comparable. The G_0W_0 spectroscopic factors behave largely like the $\Sigma^{(2)}(G)$ ones, i.e., about 0.95 for the ionization state, and somewhat smaller for the next shells. For the $3s$ orbital in Ar and the $4s$ orbital in Kr the strength of the main fragment is only about 0.5, but sizeable fragments are experimentally seen at somewhat higher energies. This fragmentation of sp strength is not reproduced in the calculations.

In our calculations the addition poles of the propagators are all at positive energy, i.e., we do not find stable $N+1$-electron (anion) states. This is in agreement with the experimental situation for the closed-(sub)shell atoms under consideration, for which the electron affinity is either zero or exceedingly small (in case of Ca). A more stringent test of the addition part of the G_0W_0 propagator would be for open-shell atoms having stable anion states [29]. However, a quasiexact treatment of the continuum is much harder to achieve than for the closed-shell atoms in the present work.

The correlation energies are presented in Table VI, where G_0W_0 results are compared with the other schemes. Note again the close correspondence between MP(2) and $\Sigma^{(2)}(G)$. On the whole, the G_0W_0 correlation energies are worse than the $\Sigma^{(2)}(G)$ results, but better than $\Sigma^{(2)}(G_{\mathrm{HF}})$. Fo r the heavier atoms (Zn and Kr), the G_0W_0 values for the correlation energy are unphysical, i.e., the G_0W_0 total energy lies above the HF one. The effect is also observed for the non-self-consistent second-order self-energy$\Sigma^{(2)}(G_{\mathrm{HF}})$,

TABLE V. Single-particle properties generated by different self-energies, compared with experimental values. All energies in atomic units. The experimental energies and occupation numbers are taken from Refs. [49–52] for the valence states (indicated with *) and from Ref. [53] for the core orbitals. Extrapolation bounds for the G_0W_0 ionization energies of He through Ar are given in Table IV.

		Single particle energies				Spectral strength		
		HF	$\Sigma^{(2)}(G)$[28]	G_0W_0	Expt.	$\Sigma^{(2)}(G)$[28]	G_0W_0	Expt.
He	1*s*	−0.918	−0.906	−0.9089	−0.9037*	0.972	0.956	
Be	1*s*	−4.732	−4.620	−4.609	−4.533*	0.873	0.895	
	2*s*	−0.309	−0.320	−0.3367	−0.343*	0.950	0.938	
Ne	1*s*	−32.77	−31.51/−33.26	−32.14	−31.70	0.544/0.364	0.852	
	2*s*	−1.931	−1.750	−1.774	−1.782*	0.876	0.905	0.85(2)
	2*p*	−0.850	−0.763	−0.801	−0.793*	0.904	0.943	0.92(2)
Mg	1*s*	−49.03	−48.20	−48.35	−47.91	0.871	0.901	
	2*s*	−3.768	−3.815/−3.399	−3.626/−3.547	−3.26	0.503/0.442	0.184/0.641	
	2*p*	−2.282	−2.146	−2.171	−2.12*	0.882	0.901	
	3*s*	−0.253	−0.274	−0.281	−0.2811*	0.962	0.941	
Ar	1*s*	−118.6	−118.0	−117.6	−117.87	0.935	0.898	
	2*s*	−12.32	−11.93	−11.95	−12.00	0.897	0.729	
	2*p*	−9.570	−9.519	−9.269	−9.160	0.786	0.898	
	3*s*	−1.277	−1.159	−1.156	−1.075*	0.876	0.858	0.55(1)
	3*p*	−0.590	−0.585	−0.595	−0.579*	0.938	0.942	0.95(2)
Ca	1*s*	−149.4		−148.5	−148.4		0.910	
	2*s*	−16.82		−16.56/−16.44/−16.28	−16.11		0.278/0.151/0.326	
	2*p*	−13.63		−13.27	−12.79		0.854	
	3*s*	−2.245		−2.073	(−1.63)		0.767	
	3*p*	−1.340		−1.314	−1.265*		0.890	
	4*s*	−0.195		−0.224	−0.225*		0.938	
Zn	1*s*	−353.3		−352.3	−355.0		0.892	
	2*s*	−44.36		−43.58	−43.96		0.610	
	2*p*	−38.92		−38.20	−37.83		0.861	
	3*s*	−5.636		−5.280	−5.14		0.676	
	3*p*	−3.836		−3.517/−3.491	−3.29		0.616/0.146	
	3*d*	−0.779		−0.646	−0.636*		0.905	
	4*s*	−0.291		−0.331	−0.345*		0.948	
Kr	1*s*	−520.2	−518.6	−519.0	−526.75	0.879	0.910	
	2*s*	−69.91	−68.67	−69.08/−68.95/−68.90	−70.63	0.861	0.221/0.347/0.113	
	2*p*	−63.01	−61.87	−62.62/−62.07	−62.356	0.883	0.112/0.743	
	3*s*	−10.85	−10.14	−10.53/−10.42	−10.77	0.729	0.129/0.388	
	3*p*	−8.332	−7.756	−7.959	−7.979	0.793	0.787	
	3*d*	−3.824	−3.566	−3.598	−3.47*	0.901	0.908	
	4*s*	−1.153	−1.119	−1.054	−1.012*	0.933	0.843	0.510(6)
	4*p*	−0.524	−0.560	−0.536	−0.519*	0.960	0.944	0.980(5)

but disappears when the self-energy $\Sigma^{(2)}(G)$ is calculated self-consistently (see Kr), suggesting that it is inherent for a non-self-consistent treatment of the self-energy.

V. BUILDING A G_0W_0-BASED FUNCTIONAL

A. General considerations

In general, the single-particle spectral function of an interacting system is related to the propagator as

$$S(\alpha,\beta;E) = \frac{1}{2\pi i}\,\mathrm{sign}(\epsilon_F - E)[G(\alpha,\beta;E) - G^*(\beta,\alpha;E)], \tag{18}$$

where the Fermi energy for finite systems can be defined as $\epsilon_F = \frac{1}{2}(E_0^{N+1} - E_0^{N-1})$. The zeroth and first energy-weighted moments obey the sum rules

TABLE VI. Correlation energies (a.u.) for different schemes. In the first row, the HF ground-state energy is given. See caption of Table V for the labeling of the other rows. Extrapolation bounds are given between brackets. The experimental values are taken from Ref. [48].

	He	Be	Ne	Mg	Ar	Ca	Zn	Kr
HF energy	−2.862	−14.573	−128.547	−199.615	−526.818	−676.758	−1777.848	−2752.055
MP(2)	−0.0368 [−0.0374,−0.0372]	−0.0615 [−0.0745,−0.0730]	−0.338 [−0.389,−0.369]	−0.331 [−0.446,−0.383]	−0.592 [−0.713,−0.655]	−0.529	−0.851	−1.185
$\Sigma^{(2)}(G_{\mathrm{HF}})$	−0.0360 [−0.0356,−0.0344]	−0.0602 [−0.0652,−0.0640]	−0.162 [−0.1594,−]	−0.132 [−0.159,−0.154]	−0.245	−0.018	0.888	0.559
$\Sigma^{(2)}(G)$[28]	−0.037	−0.055	−0.339	−0.331	−0.596			−1.135
G_0W_0	−0.065 [−0.061]	−0.101 [−0.115,−0.114]	−0.276 [−0.298,−0.290]	−0.232	−0.420	−0.192	0.317	0.143
Expt.	−0.042	−0.094	−0.391	−0.439	−0.726			

$$N_{\alpha,\beta} = \int_{-\infty}^{+\infty} dES(\alpha,\beta;E) = \langle \Psi_0^N | \{a_\beta^\dagger, a_\alpha\} | \Psi_0^N \rangle,$$

$$M_{\alpha,\beta} = \int_{-\infty}^{+\infty} dEES(\alpha,\beta;E) = \langle \Psi_0^N | \{a_\beta^\dagger, [a_\alpha, \hat{H}]\} | \Psi_0^N \rangle. \tag{19}$$

Note that the integrations in Eq. (19) are over the entire energy axis. If the integration is restricted to the removal domain $(-\infty, \epsilon_F)$ one retrieves the one-body density matrix $[N^{(-)}]$ and removal energy matrix $[M^{(-)}]$ as defined in Eqs. (14), i.e.,

$$N_{\alpha,\beta} = \int_{-\infty}^{\epsilon_F} dES(\alpha,\beta;E) + \int_{\epsilon_F}^{+\infty} dES(\alpha,\beta;E) = N_{\alpha,\beta}^{(-)} + N_{\alpha,\beta}^{(+)}, \tag{20}$$

and similarly for $M_{\alpha,\beta}$.

Working out the (anti)commutators on the right-hand side of Eq. (19), the sum rules can be expressed in closed form as

$$N_{\alpha,\beta} = \delta_{\alpha,\beta}, \tag{21}$$

$$M_{\alpha,\beta} = \langle \alpha | H_0 | \beta \rangle + \sum_{\gamma\delta} \langle \alpha\gamma | V | \beta\delta \rangle_{as} N_{\delta\gamma}^{(-)}. \tag{22}$$

In normal Fermi systems, the bulk of the spectral strength is concentrated in quasiparticle states, which (at least near the Fermi surface) can be thought of as the solutions of

$$\{[H_0] + \mathrm{Re}[\Sigma(E)]\}u = Eu. \tag{23}$$

In the closed-shell systems at hand, e.g., the first ionization state Ψ_0^{N-1} (corresponding to the first pole in the removal domain of the propagator) typically has a spectroscopic factor of about 95% (see Table V). More deeply bound orbitals may acquire a width, but have similar summed strength concentrated near an average quasiparticle energy.

One can therefore consider to split off the quasiparticle part of the spectral function,

$$[S(E)] = [S_Q(E)] + [S_B(E)], \tag{24}$$

and try to parametrize the residual small background contribution. Since the dependence on the external potential is mostly absorbed in the quasiparticle part, the background part can be assumed to be generated only by universal electron-electron correlations.

In fact, the full energy dependence of $[S_B(E)]$ is not needed, since one can apply the quasiparticle-background separation of Eq. (24) to the energy integrations in Eq. (19), i.e., one has

$$[N] = [N_Q] + [N_B], \quad [M] = [M_Q] + [M_B], \quad \text{etc.} \tag{25}$$

It is now clear that modelling the background contributions $[M_B^{(\pm)}]$ and $[N_B^{(\pm)}]$ as a functional of, e.g., the density matrix $[N^{(-)}]$, is sufficient to generate a self-consistent set of equations. Using Eqs. (21) and (25) the eigenvalue problem $[M_Q]u = \lambda[N_Q]u$, determining the quasiparticle orbitals and energies, can be expressed as

$$([M] - [M_B])u = \lambda([I] - [N_B])u. \tag{26}$$

The N solutions with lowest energy represent excitations in the $N-1$ system, and contribute to the density matrix.

A detailed discussion of this procedure, and its relation to DFT, will be given in a future presentation [54]. Here we merely want to demonstrate the feasibility of such an approach, by reproducing the G_0W_0 results of Sec. IV.

B. Background separation in the spectral function

Since we have assumed the G_0W_0 propagator to be diagonal in the HF basis, the same holds for the spectral function $S_\alpha(E)$. The contribution of the quasiparticle and background components to the $N_\alpha^{(\pm)}$ and $M_\alpha^{(\pm)}$ integrals is most easily obtained by replacing the propagator by a three-pole ansatz. One pole at energy $\epsilon_{Q\alpha}$ and with strength $s_{Q\alpha}$ should describe the quasiparticle excitation. The two other poles, at $\epsilon_{B\alpha}^{(\pm)}$ and with strength $s_{B\alpha}^{(\pm)}$, reflect the background in the removal and addition domain. Note that this ansatz is the same as used in Refs. [28,29,33] to simplify the intermediate propagator in fully self-consistent calculations.

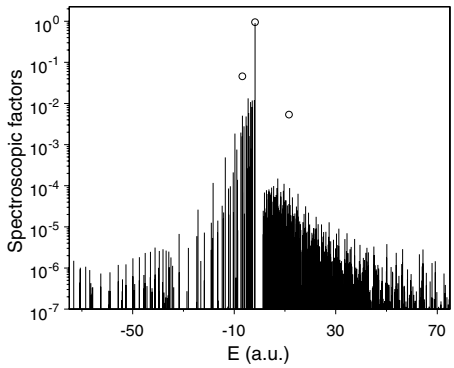

FIG. 6. The G_0W_0 spectral function of the $2s$ orbital in Ne, represented as a bar diagram. The location and strength of the poles in the three-pole ansatz are depicted as open circles.

The position and strength of the three poles should be chosen in such a way that the zeroth and first energy-weighted moments of the *ab initio* (G_0W_0) spectral function are reproduced, in both the removal and addition domain. This requirement is sufficient to determine one of the background poles, e.g., for a hole state $\alpha \equiv h$ the quasiparticle pole is in the removal domain, and in the addition domain one simply has

$$s_{Bh}^{(+)} = \int_{\epsilon_F}^{+\infty} dES_h(E), \quad s_{Bh}^{(+)}\epsilon_{Bh}^{(+)} = \int_{\epsilon_F}^{+\infty} dEES_h(E). \quad (27)$$

In the removal domain the quasiparticle-background splitting is somewhat ambiguous, but one must have at least that

$$s_{Bh}^{(-)} + s_{Qh} = \int_{-\infty}^{\epsilon_F} dES_h(E), \quad s_{Bh}^{(-)}\epsilon_{Bh}^{(-)} + s_{Qh}\epsilon_{Qh} = \int_{-\infty}^{\epsilon_F} dEES_h(E). \quad (28)$$

A choice of two more constraints is needed to fix the two poles, keeping in mind that near the Fermi energy the quasiparticle pole should be very close to the well-defined quasiparticle pole of the *ab initio* spectral function. While the remainder of the analysis does not depend on the precise choice, we find that good results are obtained by requiring the reproduction of two additional energy-weighted moments. As an example, Fig. 6 shows the G_0W_0 spectral function and the three-pole ansatz for the $2s$ orbital in Ne.

The matrices $[N_B^{(\pm)}]$ and $[M_B^{(\pm)}]$ corresponding to the present *ab initio* model are now completely known: they are diagonal and given by $N_{B\alpha}^{(\pm)} = s_{B\alpha}^{(\pm)}$, $M_{B\alpha}^{(\pm)} = s_{B\alpha}^{(\pm)}\epsilon_{B\alpha}^{(\pm)}$, respectively.

C. Modelling the background contribution

The G_0W_0 self-energy (a non-self-consistent approach) is evaluated with HF propagators. The corresponding spectral function therefore has the properties

$$\int dES_\alpha(E) = 1, \quad \int dEES_\alpha(E) = \epsilon_\alpha^{\mathrm{HF}}. \quad (29)$$

To be consistent the general Eq. (26), that generates a self-consistency problem through the dependence of $[M]$ on the density matrix, should be solved in first iteration as a correction starting from the HF picture. The first moment $[M]$ appearing in the general Eq. (26) must therefore be evaluated with the HF density matrix, and reduces to the HF Hamiltonian. Taking into account the diagonal approximation, the eigenvalue problem of Eq. (26) becomes an algebraic equation

$$\epsilon_\alpha^{\mathrm{HF}} - s_{B\alpha}^{(+)}\epsilon_{B\alpha}^{(+)} - s_{B\alpha}^{(-)}\epsilon_{B\alpha}^{(-)} = \epsilon_{Q\alpha}s_{Q\alpha} \quad (30)$$

(with $s_{Q\alpha} = 1 - s_{B\alpha}^{(+)} - s_{B\alpha}^{(-)}$), which is indeed fulfilled as it is equivalent with Eq. (29).

In principle, the modelling of the background quantities now amounts to finding a functional for $(s_{B\alpha}^{(\pm)}, \epsilon_{B\alpha}^{(\pm)})$ in terms of HF quantities. This would then yield the $(s_{Q\alpha}, \epsilon_{Q\alpha})$ and hence the first two energy-weighted moments of the spectral function in the removal and addition domain. However, with the eye on future applications it would be highly impractical to model (s_{Qp}, ϵ_{Qp}) for individual *virtual* orbitals, since it would lead to severe basis-set dependence. In the following we will therefore consider only the summed contributions of the virtual orbitals, to the correlation energy.

The correlation energy $\Delta\mathcal{E} = E_0^N(G_0W_0) - E_0^N(\mathrm{HF})$ can be written, according to the Migdal-Galitskii sum rule, as

$$\begin{aligned}\Delta\mathcal{E} &= \frac{1}{2}\Bigg(\sum_h \langle h|H_0|h\rangle(s_{Qh} + s_{Bh}^{(-)} - 1) + \sum_p \langle p|H_0|p\rangle s_{Bp}^{(-)} \\ &\quad + \sum_h (s_{Qh}\epsilon_{Qh} + s_{Bh}^{(-)}\epsilon_{Bh}^{(-)} - \epsilon_h^{\mathrm{HF}}) + \sum_p s_{Bp}^{(-)}\epsilon_{Bp}^{(-)}\Bigg) \\ &= \frac{1}{2}\Bigg(\sum_p \langle h|H_0|h\rangle s_{Bp}^{(-)} - \sum_h \langle p|H_0|p\rangle s_{Bh}^{(+)} + \sum_p s_{Bp}^{(-)}\epsilon_{Bp}^{(-)} \\ &\quad - \sum_h s_{Bh}^{(+)}\epsilon_{Bh}^{(+)}\Bigg). \end{aligned} \quad (31)$$

The last line is obtained using Eq. (30) and only contains background $p(-)$ and $h(+)$ poles, i.e., it does not depend on the precise description of the quasiparticle-background separation.

It is convenient to rewrite the correlation energy as a sum of three terms with definite sign,

$$\Delta\mathcal{E} = \tfrac{1}{2}(\Delta_0 + B^{(+)} + B^{(-)}), \quad (32)$$

where

$$\Delta_0 = \sum_p \langle h|H_0|h\rangle s_{Bp}^{(-)} - \sum_h \langle p|H_0|p\rangle s_{Bh}^{(+)} > 0,$$

$$B^{(-)} = -\sum_p s_{Bp}^{(-)}(\epsilon_F - \epsilon_{Bp}^{(-)}) < 0,$$

$$B^{(+)} = -\sum_h s_{Bh}^{(+)}(\epsilon_{Bh}^{(+)} - \epsilon_F) < 0. \quad (33)$$

The first term is positive (provided $\langle h|H_0|h\rangle < \langle p|H_0|p\rangle$, which is usual in a normal Fermi system), and represents the energy increase of the unperturbed Hamiltonian due to the depletion of the hole states and occupation of the particle states. The second and third term are negative, since the

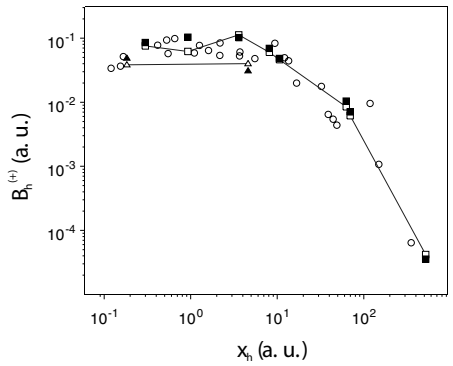

FIG. 7. Contributions of individual hole orbitals to $B^{(+)}$ versus $x_h=\epsilon_F-\epsilon_h^{\mathrm{HF}}$ for all atoms. The open symbols represent the G_0W_0 values of $B_h^{(+)}$ [see Eq. (35)]. The points corresponding to the two Be orbitals (triangles) and the eight Kr orbitals (squares) are connected by a line. The corresponding solid symbols represent the values for Be and Kr given by the functional in Eq. (36).

$\epsilon^{(+)}$ ($\epsilon^{(-)}$) are located above (below) the Fermi energy. Note that Eq. (32) follows from Eq. (31) by using particle-number conservation, $\Sigma_p s_{Bp}^{(-)}=\Sigma_h s_{Bh}^{(+)}$. The G_0W_0 self-energy slightly violates this (the maximal relative deviation is 2×10^{-3} for Be), but the difference for the correlation energy is less than 1 mH.

We now discuss the separate modelling of the three terms in Eq. (33). For the $B^{(+)}$ term, the individual $B_h^{(+)}=s_{Bh}^{(+)}(\epsilon_{Bh}^{(+)}-\epsilon_F)$ corresponding to the occupied orbitals in all atoms are represented by the open symbols in Fig. 7, as a function of $x_h=\epsilon_F-\epsilon_h^{\mathrm{HF}}$. Since the HF spectrum for the particle states starts at zero energy, the HF Fermi energy is taken as $\epsilon_F=\frac{1}{2}\epsilon_{h_I}^{\mathrm{HF}}$, with h_I the ionization orbital. The *ab initio* data points in Fig. 7 follow a global behavior as a function of x, with the reasonable limit that correlation effects become negligible for orbitals corresponding to deeply bound electrons. A similar global behavior is observed in Fig. 8, where the $B_h^{(+)}$ are plotted versus the average density of the HF orbital,

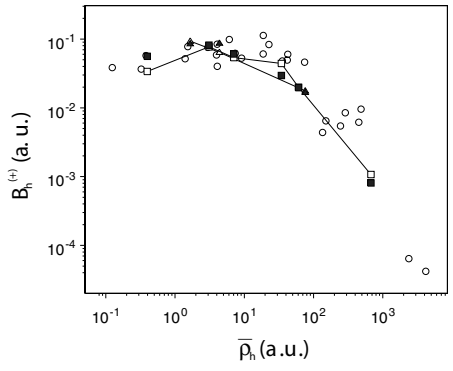

FIG. 8. Contributions of individual hole orbitals to $B^{(+)}$ versus $\bar{\rho}_h$ for all atoms. The open symbols represent the G_0W_0 values of $B_h^{(+)}$ [see Eq. (35)]. The points corresponding to the three Ne orbitals (triangles) and the six Ca orbitals (squares) are connected by a line. The corresponding solid symbols represent the values for Ne and Ca given by the functional in Eq. (36).

TABLE VII. Optimized parameter set for the functional in Eqs. (36)–(39).

	C	a	b	c
(+)	0.0993	−0.4958	0.4564	0.4200
0	0.1591	−1.5215	1.3938	−0.0817
(−)	0.0249	−0.3630	−0.1078	1.0149
I	0.8039	0.5644	0.3154	−0.3483

$$\bar{\rho}_h=\int d\mathbf{r}\rho(\mathbf{r})|\phi_h(\mathbf{r})|^2, \tag{34}$$

with correlation effects decreasing for high densities. Both trends are related, of course, but we found it useful, especially for orbitals near the Fermi surface, to keep both the dependence on x_h and on $\bar{\rho}_h$. Looking at data points (connected by lines in Figs. 7 and 8) of orbitals in the same atom, it is clear that a function of x_h and $\bar{\rho}_h$ can only describe the average behavior, and considerable scatter is observed. This could be expected in atoms where details of the allowed angular-momentum couplings are important (and should be less in complex molecules). The final interest, however, lies in the reproduction of the correlation energy which only contains the summed contribution of orbitals.

Visual inspection of the data suggested that the average behavior of the *ab initio* data points is adequately represented by a simple functional dependence,

$$B_h^{(+)}=s_{Bh}^{(+)}(\epsilon_F-\epsilon_{Bh}^{(+)})\sim f(x_h,\bar{\rho}_h)=e^{-\sqrt{x_h}/3}(\bar{\rho}_h)^{-2/3}\frac{x_h}{\sqrt{1+x_h}}, \tag{35}$$

to which an atom-dependent proportionality factor should be added. For the $B^{(+)}$ term in Eq. (33) we therefore propose

$$B^{(+)}=-\left[\mathcal{C}^{(+)}(-\epsilon_{h_I}^{\mathrm{HF}})^{a^{(+)}}(\bar{\rho}_{h_I})^{b^{(+)}}(-\epsilon_{h_I}^{(0)})^{c^{(+)}}\right]\sum_h f(x_h,\bar{\rho}_h), \tag{36}$$

where the bracketed proportionality factor is expressed as a power law in three HF variables characterizing the atomic

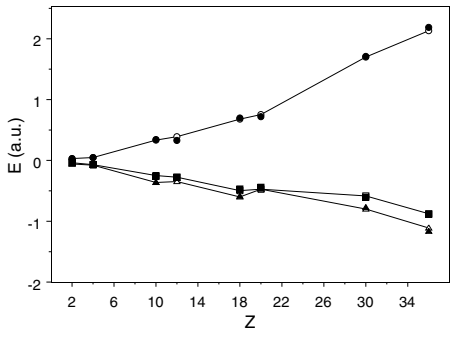

FIG. 9. The three contributions of Eq. (33) to the G_0W_0 correlation energy $\Delta\mathcal{E}$ versus atomic number Z. The open symbols, connected by a line, represent the G_0W_0 values. The corresponding closed symbols depict the values from the functional in Eqs. (36)–(38). Circles, $\frac{1}{2}\Delta_0$; squares, $\frac{1}{2}B^{(+)}$; and triangles, $\frac{1}{2}B^{(-)}$.

TABLE VIII. Comparison between the G_0W_0 values for the three energy terms in Eq. (33), the total correlation energy $\Delta\mathcal{E}$, and the shift in ionization energy $\epsilon_{Qh_I}-\epsilon_{h_I}^{\mathrm{HF}}$, with values from the functional as defined in Eqs. (36)–(39).

	G_0W_0					Functional				
	$\frac{1}{2}\Delta_0$	$\frac{1}{2}B^{(+)}$	$\frac{1}{2}B^{(-)}$	$\Delta\mathcal{E}$	$\epsilon_{Qh_I}-\epsilon_{h_I}^{\mathrm{HF}}$	$\frac{1}{2}\Delta_0$	$\frac{1}{2}B^{(+)}$	$\frac{1}{2}B^{(-)}$	$\Delta\mathcal{E}$	$\epsilon_{Qh_I}-\epsilon_{h_I}^{\mathrm{HF}}$
He	0.031	−0.057	−0.038	−0.065	−0.0090	0.029	−0.058	−0.037	−0.065	−0.0106
Be	0.048	−0.079	−0.070	−0.101	0.0278	0.048	−0.080	−0.073	−0.105	0.0280
Ne	0.334	−0.362	−0.249	−0.276	−0.049	0.345	−0.361	−0.263	−0.279	−0.040
Mg	0.391	−0.347	−0.276	−0.232	0.028	0.330	−0.298	−0.277	−0.245	0.030
Ar	0.678	−0.601	−0.497	−0.420	0.005	0.699	−0.588	−0.470	−0.359	−0.006
Ca	0.755	−0.472	−0.473	0.143	0.012	0.718	−0.471	−0.442	0.139	0.011
Zn	1.700	−0.799	−0.583	−0.192	0.029	1.709	−0.774	−0.605	−0.194	0.034
Kr	2.131	−1.111	−0.877	0.317	0.040	2.188	−1.164	−0.884	0.330	0.040

system near the Fermi energy: the HF particle-hole gap $(-\epsilon_{h_I}^{\mathrm{HF}})$, the average density $\bar{\rho}_{h_I}$, and the unperturbed energy $\epsilon_{h_I}^{(0)}=\langle h_I|\hat{H}_0|h_I\rangle$ of the ionization orbital.

For the terms $B^{(-)}$ and Δ_0, which contain contributions of the virtual orbitals, the same power-law form is used,

$$B^{(-)}=-[\mathcal{C}^{(-)}(-\epsilon_{h_I}^{\mathrm{HF}})^{a^{(-)}}(\bar{\rho}_{h_I})^{b^{(-)}}(-\epsilon_{h_I}^{(0)})^{c^{(-)}}]\left(\sum_h f(x_h,\bar{\rho}_h)\right), \tag{37}$$

$$\Delta_0=[\mathcal{C}_0(-\epsilon_{h_I}^{\mathrm{HF}})^{a_0}(\bar{\rho}_{h_I})^{b_0}(-\epsilon_{h_I}^{(0)})^{c_0}]\left(\sum_h f(x_h,\bar{\rho}_h)\right). \tag{38}$$

The presence of the factor $[\Sigma_h f(x_h,\bar{\rho}_h)]$ noticeably enhances the power-law goodness of fit for these terms.

Finally the G_0W_0 ionization energy, relative to the HF Fermi energy, also has definite sign and is likewise expressed as

$$\epsilon_F-\epsilon_{Qh_I}=[\mathcal{C}_I(-\epsilon_{h_I}^{\mathrm{HF}})^{a_I}(\bar{\rho}_{h_I})^{b_I}(-\epsilon_{h_I}^{(0)})^{c_I}]. \tag{39}$$

The parameter values obtained by a fit to the G_0W_0 data are listed in Table VII. The 16 model parameters were determined by Monte Carlo optimization using a cost function with equal weight contributions from the partial energies $B^{(\pm)}$ and Δ_0, the total correlation energy $\Delta\mathcal{E}$, and the ionization energy ϵ_{Qh_I}. This was done for a training set of seven atoms, all except Mg which is used as a test for the parametrization.

The G_0W_0 data are compared with the results of the functional in Figs. 9 and 10 and Table VIII. The trend for the partial energies in Fig. 9 is obviously very well reproduced, with a maximal relative deviation of less than 7% for the atoms in the training set, and 16% for Mg. The total correlation energy in Fig. 10 results from a delicate cancellation of partial energies with different signs, but the functional performs again very well. Note that it is easy to obtain near perfect fits for just the total correlation energy, but we feel that it has physical importance to capture the competition between the three partial energies as well. The largest deviation in the correlation energy does not occur for the test atom but for Ar. This is understandable, since the functional is required to reproduce the unphysical trend in the G_0W_0 correlation energies, which rise and become positive for the heavier atoms. Since the functional seems to have sufficient flexibility to do this, one can certainly expect accurate results for more realistic *ab initio* models. Figure 10 also contains the shift in ionization energy from its HF value, which is also nicely captured by the functional.

Another feature, visible in the partial energies of Fig. 9 and even more pronounced in the correlation and ionization energies of Fig. 10, is the staggering between the noble gas atoms and the alkaline earth atoms, with the *s* subshell closure in the latter leading to larger correlation effects. The built-in dependence on the HF *ph* gap in the functional, is crucial in this respect, as it can distinguish between the noble gases and the alkaline-earth series. It is gratifying to see that the functional is able to put both the correlation and ionization energy for Mg (not included in the training set) at exactly the right position within this trend.

VI. SUMMARY AND CONCLUSIONS

In this paper we studied a specific model for the electron self-energy to obtain an *ab initio* spectral function for a se-

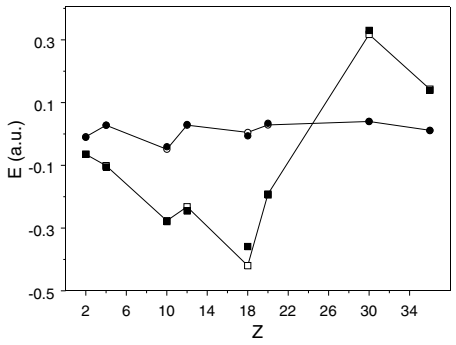

FIG. 10. The G_0W_0 shift in total and ionization energy versus atomic number Z. The open symbols, connected by a line, represent the G_0W_0 values. The corresponding closed symbols depict the values of the functional. Circles, shift in ionization energy $\epsilon_{Qh_I}-\epsilon_{h_I}^{\mathrm{HF}}$; squares, correlation energy $\Delta\mathcal{E}$.

ries of test systems, consisting of the closed-shell atoms He, Be, Ne, Mg, Ar, Ca, Zn, and Kr. For the self-energy the G_0W_0 approximation was taken. This leads to good values for the ionization energies, somewhat better than the second-order self-energy, even in the self-consistent version. The G_0W_0 correlation energy, however, becomes unrealistic for the larger atoms.

The inclusion of exchange in the polarization propagator leads to a realistic spectrum of excited states, but only for the noble gases. For atoms with a smaller *ph* gap, the RPA including exchange has instabilities, or leads to very small excitation energies.

In the future we intend to perform similar studies for molecular systems. Note that the use of pseudopotential methods while restricting to the valence electrons, can be easily incorporated in a GF framework.

The present work is part of a program that aims at constructing functionals for the correlation part of the electronic spectral function. A brief outline is given of the underlying general theory, which leads to single-particle equations describing the quasiparticle energies and orbitals. More details concerning the potential exactness of such an approach, will be provided elsewhere [54]. In this paper we constructed a simple functional that depends only on HF quantities, but is able to reproduce the effects of electron correlations embedded in the G_0W_0 self-energy. Instead of focusing solely on the correlation energy, we require that several partial contributions to the correlation energy, as well as the ionizaton energy, are simultaneously reproduced. In this way, one can expect to obtain a more realistic description of correlated electronic systems.

ACKNOWLEDGMENTS

One of the authors (P.W.A.) acknowledges support from NSERC and the Canada Research Chairs, S.V. from the Research Council of Ghent University.

[1] W. Kohn and L. J. Sham, Phys. Rev. **140**, A1133 (1965).
[2] P. Hohenberg and W. Kohn, Phys. Rev. **136**, B864 (1964).
[3] Y. Zhang and W. Yang, J. Chem. Phys. **109**, 2604 (1998).
[4] O. V. Gritsenko, B. Ensing, P. R. T. Schipper, and E. J. Baerends, J. Phys. Chem. A **104**, 8558 (2000).
[5] A. D. Becke, J. Chem. Phys. **119**, 2972 (2003).
[6] J. Grafenstein and D. Cremer, Mol. Phys. **103**, 279 (2005).
[7] K. Molawi, A. J. Cohen, and N. C. Handy, Int. J. Quantum Chem. **89**, 86 (2002).
[8] A. J. Cohen and N. C. Handy, Mol. Phys. **99**, 607 (2001).
[9] N. C. Handy and A. J. Cohen, Mol. Phys. **99**, 403 (2001).
[10] A. Görling and M. Levy, Phys. Rev. A **50**, 196 (1994).
[11] A. Görling, J. Chem. Phys. **123**, 062203 (2005).
[12] G. E. Scuseria and V. N. Staroverov, in *Theory and Applications of Computational Chemistry: The First 40 Years*, edited by C. E. Dijkstra, G. Frenking, K. S. Kim, and G. E. Scuseria (Elsevier, Amsterdam, 2005), Chap. 24.
[13] I. Grabowski, S. Hirata, S. Ivanov, and R. J. Bartlett, J. Chem. Phys. **116**, 4415 (2002).
[14] R. J. Bartlett, I. Grabowski, S. Hirata, and S. Ivanov, J. Chem. Phys. **122**, 034104 (2005).
[15] R. J. Bartlett, V. F. Lotrich, and I. V. Schweigert, J. Chem. Phys. **123**, 062205 (2005).
[16] P. Mori-Sanchez, Q. Wu, and W. T. Yang, J. Chem. Phys. **123**, 062204 (2005).
[17] A. L. Fetter and J. D. Walecka, *Quantum Theory of Many Particle Systems* (McGraw-Hill, New York, 1971).
[18] W. H. Dickhoff and D. Van Neck, *Many-Body Theory Exposed: Propagator Description of Many Particle Quantum Mechanics* (World Scientific, Singapore, 2005).
[19] A. Beste and R. J. Bartlett, J. Chem. Phys. **120**, 8395 (2004).
[20] J. V. Ortiz, J. Chem. Phys. **103**, 5630 (1995).
[21] J. Linderberg and Y. Oehrn, *Propagators in Quantum Chemistry* (Academic, London, 1973).
[22] L. S. Cederbaum and W. Domcke, Adv. Chem. Phys. **36**, 205 (1977).
[23] G. Onida, L. Reining, and A. Rubio, Rev. Mod. Phys. **74**, 601 (2002).
[24] L. J. Holleboom and J. G. Snijders, J. Chem. Phys. **93**, 5826 (1990).
[25] J. V. Ortiz, Adv. Quantum Chem. **35**, 33 (1999).
[26] L. J. Sham and M. Schlüter, Phys. Rev. Lett. **51**, 1888 (1983).
[27] L. Hedin, Phys. Rev. **139**, A796 (1965).
[28] D. Van Neck, K. Peirs, and M. Waroquier, J. Chem. Phys. **115**, 4095 (2001).
[29] K. Peirs, D. Van Neck, and M. Waroquier, J. Chem. Phys. **117**, 4095 (2002).
[30] K. Peirs, D. Van Neck, and M. Waroquier, Phys. Rev. A **67**, 012505 (2003).
[31] U. von Barth and B. Holm, Phys. Rev. B **54**, 8411 (1996); B. Holm and U. von Barth, *ibid.* **57**, 2108 (1998); B. Holm, Phys. Rev. Lett. **83**, 788 (1999).
[32] E. L. Shirley, Phys. Rev. B **54**, 7758 (1996).
[33] Y. Dewulf, D. Van Neck, and M. Waroquier, Phys. Rev. B **71**, 245122 (2005).
[34] A. D. Becke, J. Chem. Phys. **88**, 2547 (1988).
[35] J. Schirmer, L. S. Cederbaum, and O. Walter, Phys. Rev. A **28**, 1237 (1983).
[36] M. S. Deleuze and L. S. Cederbaum, Phys. Rev. B **53**, 13326 (1996).
[37] N. E. Dahlen and R. van Leeuwen, J. Chem. Phys. **122**, 164102 (2005).
[38] D. W. Smith and O. W. Day, J. Chem. Phys. **62**, 113 (1975).
[39] M. M. Morrell, R. G. Parr, and M. Levy, J. Chem. Phys. **62**, 549 (1975).
[40] O. W. Day, Jr., Int. J. Quantum Chem. **57**, 391 (1996).
[41] R. C. Morrison and P. W. Ayers, J. Chem. Phys. **103**, 6556 (1995).
[42] E. L. Shirley, L. Mitas, and R. M. Martin, Phys. Rev. B **44**, 3395 (1991).
[43] P. H. Hahn, W. G. Schmidt, and F. Bechstedt, Phys. Rev. B **72**, 245425 (2005).

[44] R. N. Hill, J. Chem. Phys. **83**, 1173 (1985).
[45] W. Klopper, J. Chem. Phys. **102**, 6168 (1995).
[46] M. Ya. Amusia, N. A. Cherepkov, R. K. Janev, and Dj. Zivanovic, J. Phys. B **7**, 1435 (1974); M. Ya. Amusia, *Atomic Photoeffect* (Plenum Press, New York, 1990).
[47] H. P. Kelly, Phys. Rev. **136**, B896 (1964).
[48] S. J. Chakravorty, S. R. Gwaltney, E. R. Davidson, F. A. Parpia, and C. F. Fischer, Phys. Rev. A **47**, 3649 (1993).
[49] NIST Atomic Spectra Database, NIST Standard Reference Database #78, http://physics.nist.gov/PhysRefData/ASD/index.html
[50] O. Samardzic, S. W. Braidwood, E. Weigold, and M. J. Brunger, Phys. Rev. A **48**, 4390 (1993).
[51] I. E. McCarthy, R. Pascual, P. Storer, and E. Weigold, Phys. Rev. A **40**, 3041 (1989).
[52] R. Nicholson, S. W. Braidwood, I. E. McCarthy, E. Weigold, and M. J. Brunger, Phys. Rev. A **53**, 4205 (1996).
[53] A. Thompson *et al.*, *X-ray Data Booklet* (Lawrence Berkeley National Laboratory, Berkeley, CA, 2001), and references cited therein.
[54] D. Van Neck, S. Verdonck, G. Bonny, P. W. Ayers, and M. Waroquier, Phys. Rev. A **74**, 042501(2006).